

# Magnetic properties and spin polarization of $\text{Co}_2\text{MnSi}$ Heusler alloy thin films epitaxially grown on $\text{GaAs}(001)$

W. H. Wang,<sup>1,2</sup> M. Przybylski,<sup>1,3,\*</sup> W. Kuch,<sup>1,4</sup> L. I. Chelaru,<sup>1,5</sup> J. Wang,<sup>1,6</sup> Y. F. Lu,<sup>1</sup> J. Barthel,<sup>1</sup> H. L. Meyerheim,<sup>1</sup> and J. Kirschner<sup>1</sup>

<sup>1</sup>Max-Planck-Institut für Mikrostrukturphysik, Weinberg 2, 06120 Halle, Germany

<sup>2</sup>National Institute for Materials Science, 1-2-1 Sengen, Tsukuba, Ibaraki 305-0047, Japan

<sup>3</sup>Solid State Physics Department, Faculty of Physics and Applied Computer Science, AGH University of Science and Technology, Mickiewicza 30, 30-059 Krakow, Poland

<sup>4</sup>Institut für Experimentalphysik, Freie Universität Berlin, Arnimallee 14, 14195 Berlin, Germany

<sup>5</sup>Institut für Experimentelle Physik, Universität Duisburg-Essen, Universitätsstrasse 5, 45117 Essen, Germany

<sup>6</sup>Department of Physics and HKU-CAS Joint Lab on New Materials, The University of Hong Kong, Hong Kong, China

(Received 20 August 2004; published 22 April 2005)

Single-crystalline  $\text{Co}_2\text{MnSi}$  Heusler alloy films have been grown on  $\text{GaAs}(001)$  substrates by pulsed laser deposition (PLD). The best crystallographic quality of the  $\text{Co}_2\text{MnSi}$  films has been achieved after deposition at 450 K. The films exhibit in-plane uniaxial magnetic anisotropy with the easy axis of magnetization along the  $[1-10]$  direction superimposed with a fourfold anisotropy with the easy axis along  $\langle 110 \rangle$ . Spin-resolved photoemission measurements of the single-crystalline  $\text{Co}_2\text{MnSi}$  films reveal a spin-resolved density of states that is in qualitative agreement with recent band structure calculations. The spin polarization of photoelectrons close to the Fermi level is found to be at most 12%, in contrast to the predicted half-metallic behavior. We suggest that these discrepancies may be attributed to a partial chemical disorder in the  $\text{Co}_2\text{MnSi}$  lattice.

DOI: 10.1103/PhysRevB.71.144416

PACS number(s): 75.70.Rf, 68.55.-a, 75.50.Cc

## I. INTRODUCTION

It was successfully proven recently that a magnetic semiconductor based system is feasible as spin injection source<sup>1,2</sup> however, only under conditions of low temperatures and high magnetic fields.<sup>3</sup> From the practical requirement of functionality with small magnetic fields and at environmental temperatures, the concept of spin injection from a metallic ferromagnet into a semiconductor is still very attractive. Due to a recent work that imposed severe restrictions on the functionality of integrated ferromagnetic metal-semiconductor devices, this concept needs substantial modifications, e.g., by the integration of a tunnel junction to produce hot electrons as a part of the spintronic device.<sup>4-6</sup> Also “natural” polarization of the electrons at the Fermi level seems to be insufficient for an effective spin-dependent transport and a spin-valve filtering, in lack of 100% spin polarized materials, has to be applied in addition.<sup>7</sup> Finally, a nonmagnetic layer at the interface might act as a strong spin scatterer, thus losing the spin information being transferred into the semiconductor.<sup>8</sup>

Ferromagnetic materials that have Curie temperatures ( $T_c$ ) above room temperature and a high spin polarization show great promise for integration with semiconductor electronics.<sup>9</sup> It has been shown that it is possible to grow single-crystalline Fe films on  $\text{GaAs}(001)$ ,<sup>10</sup> which have been proposed for spin-polarized current injection from a metal into a semiconductor. On the other hand, half-metallic ferromagnets have been proposed as ideal candidates for spin injection devices because they have been predicted to exhibit 100% spin polarization at the Fermi level.<sup>11</sup> Notable among the half-metallic candidates are a number of the full-Heusler ( $L2_1$  structure) and half-Heusler ( $C1_b$  structure) alloys.<sup>11,12</sup> They have crystal structures and lattice parameters similar to

many semiconductors, and thus could be easily epitaxially grown on top of them. In addition, they exhibit high Curie temperature and high spin polarization at the Fermi level as predicted by theory.<sup>13</sup> These properties make them particularly attractive as injectors and detectors of the spin polarized current. The most widely studied half-Heusler alloy thin film is  $\text{NiMnSb}$ .<sup>14,15</sup> Turban *et al.*<sup>14</sup> found that the higher the growth temperature, the smaller the number of defects in the  $\text{NiMnSb}$  epitaxial layers grown on  $\text{MgO}$ . However, when  $\text{NiMnSb}$  is grown on a semiconductor, the higher deposition temperatures result in more extensive interfacial reactions that can potentially result in the formation of magnetically dead layers. Hence, a compromise must be made between the crystal quality and possible interfacial reactions. Recently, a number of Heusler alloys have been grown epitaxially on semiconductor substrates including  $\text{Co}_2\text{MnGe}$ ,<sup>16</sup>  $\text{Ni}_2\text{MnGa}$ ,<sup>17</sup> and  $\text{Ni}_2\text{MnGe}$  (Ref. 18) on  $\text{GaAs}(001)$ , and  $\text{Ni}_2\text{MnIn}$  (Ref. 19) on  $\text{InAs}(001)$ . Analyzing the growth of these full Heusler alloys, it was found that the substrate temperature has a dramatic effect on the interface reactions, crystal quality, magnetic properties, and atomic ordering. For growth above 500 K, cross-sectional transmission electron microscopy studies indicate that substantial interfacial reactions have occurred, and for growth below 400 K, a large number of textures and additional amorphous phases have been formed in the films. The optimum growth was achieved at about 450 K.

Recently, the full Heusler alloy  $\text{Co}_2\text{MnSi}$  has attracted interest because it is predicted to have a large minority spin band gap of  $\sim 0.4$  eV and has the highest Curie temperatures of 985 K among the known full and half Heusler alloys.<sup>13,20</sup> More recently, the magnetic, structural, and transport properties of  $\text{Co}_2\text{MnSi}$  have been reported for dc magnetron sputtered polycrystalline films and single crystals.<sup>21-24</sup> Very re-

cently, magnetic tunnel junctions with a magnetically soft  $\text{Co}_2\text{MnSi}$  electrode have been investigated with respect to their structural and magnetic properties.<sup>25</sup> In the bulk,  $\text{Co}_2\text{MnSi}$  has been stabilized in the cubic  $L2_1$  structure with a lattice parameter of 5.67 Å, which implies a lattice mismatch to the GaAs(001) substrate of only 0.3%. It therefore can be expected that GaAs(001) is a suitable substrate for epitaxial growth of single-crystalline  $\text{Co}_2\text{MnSi}$  films. Despite the crucial importance of preparing well characterized  $\text{Co}_2\text{MnSi}$  thin films that show a very high volume and surface crystalline quality, to the best of our knowledge, only very few experimental works have been devoted to the study of  $\text{Co}_2\text{MnSi}$  epitaxial growth and in particular its spin polarization. In this paper we present a detailed study of the growth, structural and magnetic properties, and spin polarization of single-crystalline  $\text{Co}_2\text{MnSi}$  thin films grown on GaAs(001) by PLD.

The paper is organized as follows. Experimental details are presented in Sec. II. The growth and structural study of the single-crystalline  $\text{Co}_2\text{MnSi}$  thin films is presented in Sec. III. The magnetic properties of these films are analyzed in Sec. IV. Finally, Secs. V and VI are dedicated to the x-ray magnetic circular dichroism and spin polarization study of single-crystalline  $\text{Co}_2\text{MnSi}$  thin films, respectively.

## II. EXPERIMENTAL DETAILS

The sample preparation and characterization were carried out in an ultrahigh vacuum (UHV) multichamber system equipped with molecular beam epitaxy (MBE), *in situ* reflection high-energy electron diffraction (RHEED), Auger electron spectroscopy (AES), x-ray photoemission spectroscopy (XPS), low-energy electron diffraction (LEED), scanning tunneling microscopy (STM), and *in situ* magneto-optical Kerr effect (MOKE) analytical techniques. Commercially available GaAs(001) substrates were first degassed in UHV up to about 580 °C, subsequently the substrate surface was further sputtered for 30 min at 600 °C with a 0.6 keV  $\text{Ar}^+$  ion beam, a 4  $\mu\text{A}/\text{cm}^2$  current density, at an incidence angle of 45°. After the cleaning procedure was completed, no surface impurities were detected in the AES spectra, and sharp LEED images revealed the pseudo-(4×6) surface reconstruction characteristic for the Ga-terminated GaAs(001) surface, which has been found to protect Fe films against intermixing with As and Ga.<sup>26</sup> The  $\text{Co}_2\text{MnSi}$  thin films were deposited on GaAs(001) substrates from stoichiometric polycrystalline  $\text{Co}_2\text{MnSi}$  pellet targets by the PLD method. The base pressure in the deposition chamber was less than  $5 \times 10^{-11}$  mbar. A KrF excimer laser (248 nm wavelength, 34 ns pulse length, typical pulse energy 300 mJ, and repetition rate 10 Hz) was used, and the beam was incident at an angle of 45° onto the rotating target. The growth was followed in real time by RHEED (at 15 keV beam energy with a glancing angle of about 2.5° in  $\langle 110 \rangle$  incidence). This technique allowed us to obtain the surface structure and the growth mode by recording the (00) spot intensity variation with time. The observed RHEED intensity oscillations were characteristic of a layer-by-layer growth mode (Frank–Van der Merwe growth). The RHEED patterns also allowed us to obtain

qualitative information about the surface roughness. The surface morphology was also investigated by STM at room temperature in constant current mode. MOKE loops were collected *in situ* in longitudinal geometry by using an electromagnet with a maximum field of 0.8 T.

X-ray magnetic circular dichroism (XMCD) in soft x-ray absorption and spin-resolved photoemission measurements of the  $\text{Co}_2\text{MnSi}/\text{GaAs}(001)$  samples were carried out at the UE56/2-PGM2 beamline at BESSY in Berlin. The experiments were performed on samples that were grown in the MBE laboratory in Halle. Immediately after deposition, the samples were transported under UHV conditions in our “UHV suitcase” to Berlin. During the transport a pressure of about  $4 \times 10^{-10}$  mbar was maintained. The typical time interval between the preparation of the samples and the beginning of the measurements at BESSY was about 4 h. The base pressure in the photoemission chamber was  $5 \times 10^{-11}$  mbar. Absorption spectra were recorded by directly detecting the sample current while scanning the photon energy of the 80% circularly polarized light. Photon energy resolution was set to 0.15 and 0.19 eV for absorption at the Mn and Co  $L_{2,3}$  edges, respectively. Spin resolved photoemission spectra were taken for 45° incidence of the incoming linearly *p*-polarized radiation in the plane defined by the magnetization and surface normal, and normal emission of the outgoing photoelectrons. Spectra were taken for excitation with 70 eV photon energy and 0.14 eV photon energy resolution using a cylindrical sector analyzer (Omicron CSA 300) equipped with a spin-polarization detector based on spin-polarized low-energy electron diffraction from a W(001) single crystal (Omicron SPLEED). A pass energy of 16 eV was used for the spectra presented here. The angular acceptance of photoelectrons is about  $\pm 8^\circ$ . Analyzer entrance and exit slits were set to 3 mm, resulting in an electron energy resolution of 1.0 eV. Values of the spin polarization were corrected assuming the nominal detector asymmetry function of 0.25.<sup>27</sup> A reduction of the asymmetry function by insufficient preparation of the W(001) single crystal or misalignment of the instrument would linearly influence the values of the photoelectron spin polarization of the  $\text{Co}_2\text{MnSi}$  films reported here. However, spin polarized photoemission measurements performed under identical conditions a few days before at the same beamline on a 10 ML Co film on Cu(001) yielded 35% spin polarization at about 5 eV binding energy. Since the maximum spin polarization obtained for Co/Cu(001) at photon energies of 16–24 eV is 40%,<sup>28</sup> we think that the systematic error introduced by the guess of the asymmetry function is less than 25% of our reported spin polarization values.

Both XMCD and spin-resolved photoemission measurements have been performed in magnetic remanence after a magnetic field pulse of about 50 mT along the in-plane easy axis ( $[1-10]$ ) of the thin  $\text{Co}_2\text{MnSi}$  films has been applied. Almost 100% remanent magnetization was found at room temperature for all the  $\text{Co}_2\text{MnSi}$  films independently of the thickness. This indicates that the remanent magnetic state preserves the spin alignment along the field applied before, which is important because no magnetic field has been applied during the XMCD and spin-resolved photoemission measurements.

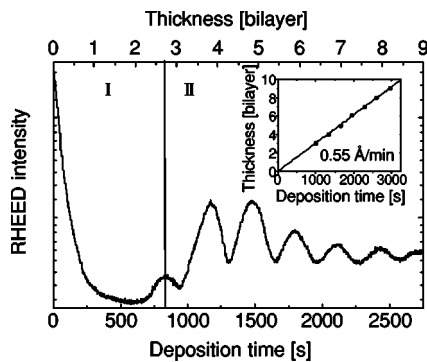


FIG. 1. RHEED intensity during growth of  $\text{Co}_2\text{MnSi}$  on  $\text{GaAs}(001)$ . The period of oscillations corresponds to two atomic layers (bilayer). In order to determine the rate of the growth, we plot in the inset the positions of maxima as a function of time.

### III. GROWTH OF $\text{Co}_2\text{MnSi}$ THIN FILMS ON $\text{GaAs}(001)$

The theoretical arguments outlined in Sec. I suggest that Heusler alloys may be ideal spin-injecting contacts to many compound semiconductors.<sup>29,30</sup> However, all experimental data show that it is difficult to grow high quality Heusler alloys on semiconductor surfaces. This is because a high deposition temperature is helpful to get a single-crystalline film, but results in extensive interfacial reactions. Hence, a compromise must be made between crystal quality and interfacial reactions. In our work, the growth of  $\text{Co}_2\text{MnSi}$  thin films was monitored by means of the RHEED oscillations. In order to suppress the interface reactions between  $\text{GaAs}$  and  $\text{Co}_2\text{MnSi}$  thin films, we have tried the growth of  $\text{Co}_2\text{MnSi}$  on the  $\text{GaAs}(001)$  at substrate temperatures as low as 475 K and below. We found that the best crystalline quality is achieved at a substrate temperature of 450 K. Figure 1 shows typical RHEED intensity oscillations as a function of deposition time (which relates directly to the film thickness), for the  $\text{Co}_2\text{MnSi}$  films grown by PLD on  $\text{GaAs}(001)$  at 450 K. It is clearly seen that the RHEED intensity does not show any oscillations at deposition of the first and second layer, instead a drop of the reflected intensity is observed. We attribute the absence of the first two oscillations to a poor layer-by-layer growth or to intermixing between the  $\text{GaAs}$  substrate and the  $\text{Co}_2\text{MnSi}$  film (as will be discussed hereafter). The regular oscillatory behavior of the RHEED intensity starts at the third layer, and it can be promoted up to about ten layers. In the case the films were grown at room temperature, no RHEED oscillations and no clear diffraction pattern after the film deposition were observed. The growth temperature of 450 K is a compromise between the epitaxy improving with increasing temperature, and intermixing in the  $\text{Co}_2\text{MnSi}/\text{GaAs}$  interface which clearly appears above 475 K.

It is interesting to find what the growth unit is in our case. The growth unit for a single-element metal or semiconductor, related to one oscillation of the RHEED spot intensity, has been confirmed to be one atomic layer. However, for the growth of some high-temperature superconducting oxides, such as  $\text{BaTiO}_3$  and  $\text{YBaCu}_3\text{O}_{7-x}$  on  $\text{SrTiO}_3(001)$  substrates, the RHEED oscillation period corresponds to one unit cell.<sup>31</sup>

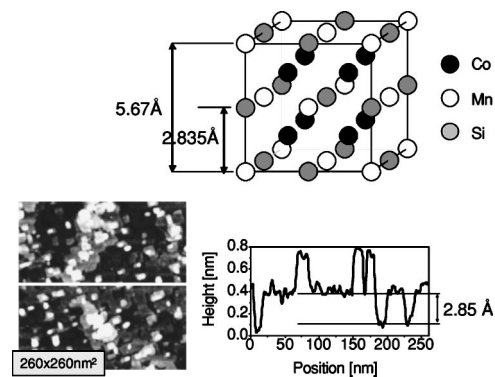


FIG. 2. STM image after deposition of five bilayers of  $\text{Co}_2\text{MnSi}$  at 450 K. The line profile taken along the solid line is shown at the right side. The roughness corresponds to 2.85 Å, i.e., one bilayer as it is shown from a sketch of the  $\text{Co}_2\text{MnSi}$  unit cell.

In order to identify the period of the RHEED oscillations, one must compare the number of the oscillations with the corresponding film thickness. For example, the thickness of the film can be determined by x-ray reflectometry.<sup>31</sup> Another method is to take STM images at different points of the RHEED oscillations to ascertain whether the maxima correspond to a full monolayer or not. Figure 2 shows a typical STM image of a  $\text{Co}_2\text{MnSi}$  thin film whose growth was stopped at the fifth peak of the RHEED oscillations. From the line profile of the image, the height of islands is found to be 2.85 Å. This value fits well to the height of half of the unit cell of  $\text{Co}_2\text{MnSi}$  (also shown in Fig. 2). It means that the RHEED oscillation period corresponds to half of the unit cell of  $\text{Co}_2\text{MnSi}$ , i.e., to the thickness of two atomic layers. This result is important for understanding the epitaxial growth of the Heusler alloys. The observed period in the RHEED oscillations indicates that the two-dimensional nuclei of  $\text{Co}_2\text{MnSi}$  all have the height of half a unit cell which is necessary to satisfy the chemical composition and electrical neutrality.

The RHEED patterns of  $\text{Co}_2\text{MnSi}$  films of varying thickness are shown in Fig. 3. The patterns are presented in two columns related to the  $[110]$  and  $[1-10]$  crystallographic directions which the electron beam is focused along. Figure 3(a) shows the pattern of the clean  $\text{GaAs}(001)$  surface before the film deposition. We note that along the  $[1-10]$  direction the reconstruction shows six lines in comparison to four lines along  $[110]$ , indicating a smooth  $(4 \times 6)$  reconstructed  $\text{GaAs}(001)$  surface. We found that the reconstruction lines in the substrate's RHEED patterns disappear immediately after the deposition of  $\text{Co}_2\text{MnSi}$  is started. At a thickness of about 6 Å (roughly 1 unit cell of  $\text{Co}_2\text{MnSi}$ ), the RHEED pattern of the underlying substrate has completely disappeared and only the new RHEED pattern from the  $\text{Co}_2\text{MnSi}$  Heusler film is seen. Furthermore, regular RHEED oscillations obtained during growth of the films thicker than 6 Å are characteristic for a layer-by-layer growth. Figure 3(b) shows the RHEED patterns obtained for a 60-Å-thick film. The principal spots coincide closely with those of the  $\text{GaAs}$  substrate along both  $[110]$  and  $[1-10]$  directions, indicating epitaxial growth. Moreover, the Kikuchi lines were clearly visible in the diffraction patterns indicating a high-quality epitaxial

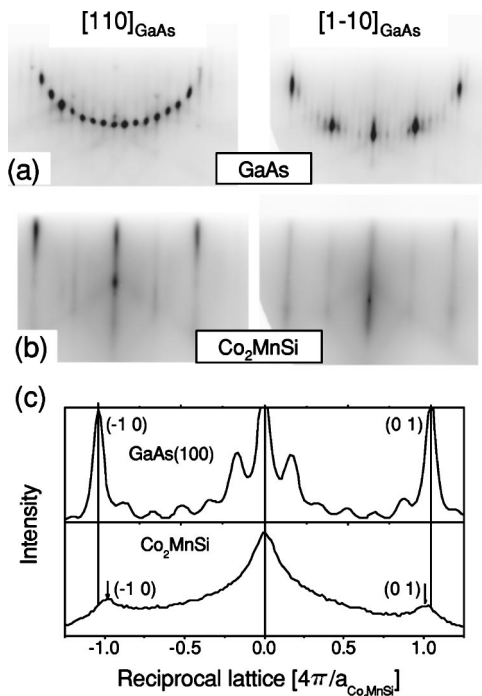


FIG. 3. RHEED patterns of (a) clean GaAs(001), (b) 60-Å-thick  $\text{Co}_2\text{MnSi}$  film, left-hand side panels along  $[110]_{\text{GaAs}}$  and right panels along  $[1-10]_{\text{GaAs}}$ , (c) line profiles of GaAs (top) and  $\text{Co}_2\text{MnSi}$  (bottom) RHEED patterns taken along  $[110]_{\text{GaAs}}$ .

single crystal film. Figure 3(c) shows profiles of the RHEED patterns along the  $[110]$  direction corresponding to GaAs and  $\text{Co}_2\text{MnSi}$  [shown in Figs. 3(a) and 3(b)]. Taking the spacing of the initial  $[1-10]$  RHEED spots for reference and using the value of 5.654 Å for GaAs, one can determine the in-plane lattice parameter of the 60-Å-thick  $\text{Co}_2\text{MnSi}$  film to be 5.67 Å from a large number of RHEED patterns. This value is in good agreement with that of the bulk single-crystalline  $\text{Co}_2\text{MnSi}$  sample.

LEED patterns of a clean GaAs(001) and after deposition of 60-Å-thick  $\text{Co}_2\text{MnSi}$  film are shown in Figs. 4(a) and 4(b), respectively, confirming epitaxial growth of the film and its rather good crystallographic order. However, no conclusion can be made on the chemical order (or disorder) based on the qualitative LEED and RHEED analysis only. It is not possible to distinguish between the ordered  $(1 \times 1)$  structure and a disordered one, where some atomic species occupy several sites within the  $(1 \times 1)$  unit cell.

In order to judge about the degree of intermixing, we performed an AES investigation of the  $\text{Co}_2\text{MnSi}$  films grown

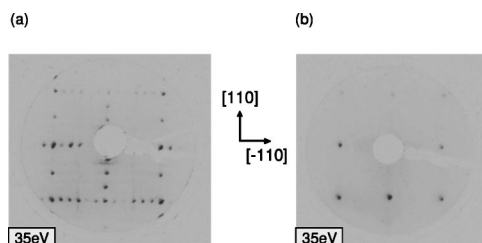


FIG. 4. LEED patterns of (a) clean GaAs(001) surface and (b) 60-Å-thick  $\text{Co}_2\text{MnSi}$  film deposited at 450 K.

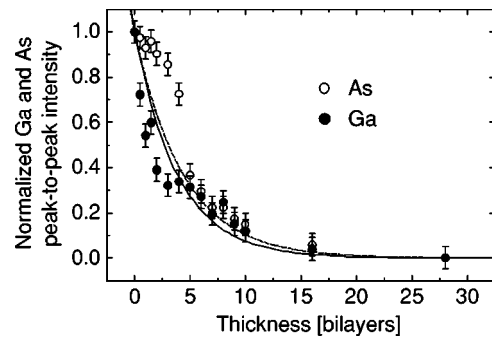


FIG. 5. AES peak-to-peak intensities of the Ga line at 1070 eV (full dots), and the As line at 1228 eV (open circles), measured for  $\text{Co}_2\text{MnSi}$  films grown at 450 K and normalized to the intensities for clean GaAs(001). The solid and dotted curves stand for the predicted Ga and As normalized intensities, respectively, under the hypothesis of an ideal  $\text{Co}_2\text{MnSi}$  growth (flat and continuous film as well as no intermixing).

at 450 K. The evolution of the Ga line at 1070 eV, the As line at 1228 eV, and the Co line at 780 eV were followed as a function of  $\text{Co}_2\text{MnSi}$  film thickness. The normalized gallium and arsenic peak-to-peak intensities are shown in Fig. 5. The normalization of the gallium and arsenic peak-to-peak intensity signals was done with respect to the Ga and As peak-to-peak intensity at zero  $\text{Co}_2\text{MnSi}$  coverage. Along with the experimental intensities, the model predicted Ga and As AES peak-to-peak intensities (normalized as before) are shown. The predicted curves were deduced by assuming an attenuation of exponential form according to

$$I^{\text{Ga,As}} = I_0^{\text{Ga,As}} \exp\left(\frac{-t_{\text{Co}_2\text{MnSi}}}{\cos \phi \cdot \lambda_{\text{Co}_2\text{MnSi}}^{\text{Ga,As}}}\right) \quad (1)$$

with inelastic mean-free paths (IMFPs) in  $\text{Co}_2\text{MnSi}$ ,  $\lambda_{\text{Co}_2\text{MnSi}}^{\text{Ga}}$  and  $\lambda_{\text{Co}_2\text{MnSi}}^{\text{As}}$  of 15 Å for the 1070 eV Ga Auger electrons,<sup>32</sup> and 17 Å for the 1228 eV As one.<sup>32-34</sup> Here,  $I_0^{\text{Ga,As}}$  stands for the substrate Ga and As intensities,  $t_{\text{Co}_2\text{MnSi}}$  is the  $\text{Co}_2\text{MnSi}$  film thickness, and  $\phi$  represents the mean opening angle of the spherical mirror analyzer. In the above approach, we supposed that the deposited  $\text{Co}_2\text{MnSi}$  forms a flat and continuous film, and no intermixing occurs at the interface. However, from a first glance at the AES signals measured for Ga (full dots in Fig. 5) and As (open circles), one can immediately see a difference between Ga and As behavior. For Ga, the experimental signal follows rather closely the predicted curve of no intermixing. However, a rather slow decay is observed for As up to 10 ML (i.e., five bilayers), followed by the predicted decay. We associate this behavior with a substantial amount of As segregating to the top of  $\text{Co}_2\text{MnSi}$  film, which gradually becomes buried into the growing film when its thickness further increases. In combination with the results of the AES analysis, we suggest that the initial lack of RHEED oscillations may be due to the intermixing between As and  $\text{Co}_2\text{MnSi}$ , which results in some crystallographic disorder in the early stages of the growth. The AES analysis shows a slightly increased signal of Mn with reference to the Co signal and to what is expected from stoichiometry of the

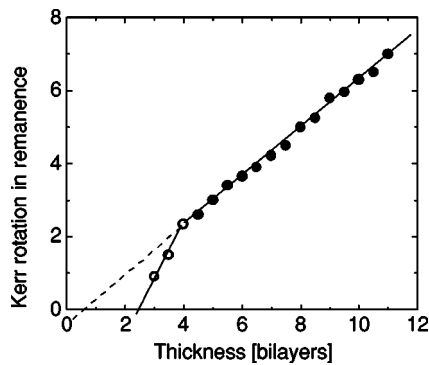


FIG. 6. Thickness dependence of longitudinal Kerr rotation measured at 70 K along the  $[1-10]$  easy-axis direction for  $\text{Co}_2\text{MnSi}$  films of varying thickness. The open dots are the results for the films thinner than four bilayers (the superparamagnetic phase) in an applied field of 0.1 T. The full dots show the saturated Kerr intensity of the ferromagnetic phase (above four bilayers), which is equivalent to the intensity in remanence in this case.

$\text{Co}_2\text{MnSi}$  compound. Due to the fact that the Mn/Co ratio exceeds the value of 0.5 (expected for the stoichiometric  $\text{Co}_2\text{MnSi}$  film) mostly for the thinnest films (below four bilayers), we suggest that Mn segregation to the surface is responsible for this effect. It is worth to mention that these first monolayers are very important for the spin polarized carrier injection into the semiconductor both from spin polarization and magnetic order point of view.

#### IV. MAGNETIC PROPERTIES

The magnetic properties of the  $\text{Co}_2\text{MnSi}$  films were probed *in situ* by magneto-optical Kerr effect (MOKE) measurements. All the films considered here were grown at 450 K. The thickness dependence of the Kerr intensity at 70 K, when the magnetization was probed along the  $[1-10]$  direction, is plotted in Fig. 6. No magnetic signal could be detected for films thinner than two bilayers ( $5.67 \text{ \AA}$ ). Just above this thickness the Kerr measurement shows a nonzero intensity in an applied field of 0.1 T, however the *s*-shaped loops do not show any hysteresis. At 70 K, for a  $\text{Co}_2\text{MnSi}$  thickness of four bilayers, a significant Kerr signal in remanence is first detected indicating the onset of ferromagnetic order. The lack of magnetic signal for the first three bilayers indicates that the ferromagnetic phase has not yet developed at 70 K. Magnetically dead layers could be expected near the  $\text{Co}_2\text{MnSi}/\text{GaAs}(001)$  interface due to atomic intermixing between the film and the substrate (As segregation, see Fig. 5). Another possibility is that a small size of the initially formed islands prevents the onset of magnetic ordering. With increasing  $\text{Co}_2\text{MnSi}$  film thickness, the islands coalesce into bigger clusters in which an internal ferromagnetic order exists at 70 K (open dots in Fig. 6). Above the thickness of four bilayers, the Kerr rotation in remanence can be plotted, which is approximately proportional to the film thickness. The remanent magnetization measured along the  $[1-10]$  easy axis gives a good estimate of the magnetic order in  $\text{Co}_2\text{MnSi}$ , in particular if it is plotted versus the film thick-

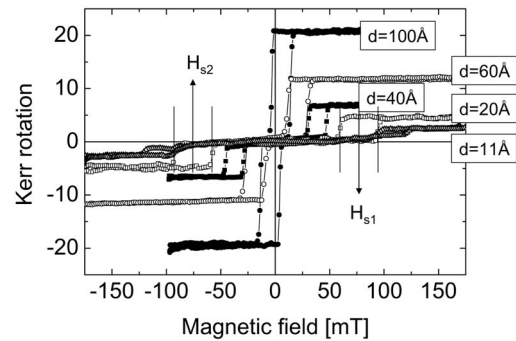


FIG. 7. Evolution of hysteresis loops of the  $\text{Co}_2\text{MnSi}/\text{GaAs}(001)$  films of varying thickness measured along the  $[110]$  hard axis direction. The switching fields  $H_{s1}$  and  $H_{s2}$ , at positive and negative fields, respectively, are defined within the figure for the  $d=20 \text{ \AA}$  thick film.

ness at low temperature. Extrapolation to zero remanence suggests that there are only 0.6 magnetically dead bilayers (Fig. 6).

An in-plane uniaxial magnetic anisotropy with the easy axis parallel to the  $[1-10]$  direction is found for thicknesses above three bilayers of  $\text{Co}_2\text{MnSi}$  deposited on  $\text{GaAs}(001)$ . This means that the ferromagnetic long-range order and uniaxial magnetic anisotropy both appear above a critical thickness of three bilayers. Figure 7 shows the evolution of the hysteresis loops measured at RT for  $\text{Co}_2\text{MnSi}$  films of varying thickness when the magnetization was probed along the  $[110]$  hard-axis direction. The uniaxial anisotropy is found to be superimposed onto the four-fold magnetic anisotropy with the easy axis of magnetization along the two  $\langle 110 \rangle$  in-plane directions. In particular, at a  $\text{Co}_2\text{MnSi}$  thickness of four bilayers, i.e.  $11 \text{ \AA}$  (see Fig. 7, open triangles), the hysteresis loop along the  $[110]$  direction splits completely into two sub-loops and the remanence becomes zero. The sub-loops are shifted to a higher magnetic field. The shift field is defined as  $H_s = (H_{s1} - H_{s2})/2$ , where  $H_{s1}$  and  $H_{s2}$  denote the fields the sub-loops are symmetric around, at positive and negative field, respectively. The hysteresis loops along the  $[110]$  direction show that the shift field depends on the  $\text{Co}_2\text{MnSi}$  film thickness  $d$ , being proportional to  $1/d$ . As shown in Fig. 7, when the thickness of  $\text{Co}_2\text{MnSi}$  film is thicker than  $100 \text{ \AA}$ , almost no clearly defined double hysteresis loops can be measured by MOKE.

Figure 8 shows a series of hysteresis loops measured at 80 K for the  $60\text{-\AA}$ -thick  $\text{Co}_2\text{MnSi}$  film along the magnetic field applied in the sample plane, under an angle  $\alpha$  in  $5^\circ$  steps with respect to the  $[1-10]$  direction. At  $\alpha=0^\circ$ , i.e., along the  $[1-10]$  direction, the loop is rectangular, clearly suggesting that it is measured along the easy-axis of magnetization. When  $\alpha$  increases from  $0^\circ$  to  $55^\circ$ , the hysteresis loops keep a rectangular shape, however the Kerr rotation in remanence decreases suggesting that the film is still magnetized along  $[1-10]$ , and only the projection of the magnetization to the field direction is detected. Interestingly, when the sample is rotated and the magnetization is probed more to the  $[110]$  direction, i.e., when  $\alpha > 60^\circ$ , the loop evolves getting a three-step character, with one loop around zero field, and two sub-loops symmetrically at positive and negative field. More-

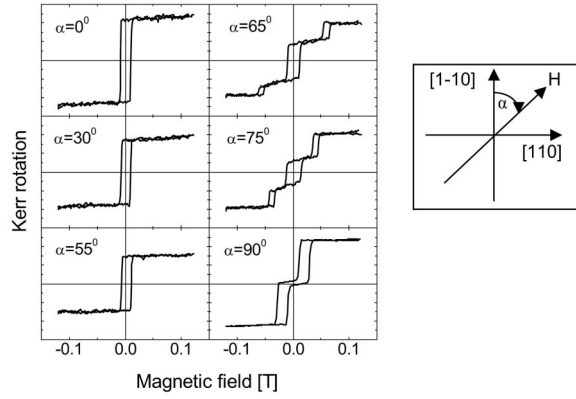


FIG. 8. Longitudinal MOKE hysteresis loops of the 60-Å  $\text{Co}_2\text{MnSi}$  film measured at 80 K along  $\alpha=0^\circ$ ,  $30^\circ$ ,  $55^\circ$ ,  $65^\circ$ ,  $75^\circ$ , and  $90^\circ$  in-plane azimuthal angle with respect to the  $[1-10]$  direction.

over, the relative contribution of the subloops to the total Kerr signal becomes more prominent when  $\alpha$  approaches  $90^\circ$ . Finally, at  $\alpha=90^\circ$ , i.e., along  $[110]$ , the central loop disappears completely and only the subloops exist. The field at which the subloops appear depends on the angle  $\alpha$  (by which the sample is rotated from the  $[1-10]$  direction) and decreases when approaching the  $[110]$  direction. When the field is applied along an intermediate direction oriented between  $[1-10]$  and  $[110]$ , field components act both along  $[1-10]$  and  $[110]$ . For the same applied field, its component along the  $[110]$  direction increases with increasing the angle  $\alpha$ . This means that the closer to the  $[110]$  direction the field is applied, the easier to reach the field which is necessary to switch the magnetization to the  $[110]$  direction. Figures 9(a) and 9(b) show diagrams illustrating how the magnetization reversal proceeds in view of the magnetization projection to the field direction for  $\alpha < 60^\circ$  and  $\alpha > 60^\circ$ , respectively. This is exactly what is measured by MOKE and reflected in the shape of the hysteresis loops. In the first case, at  $\alpha < 60^\circ$ ,

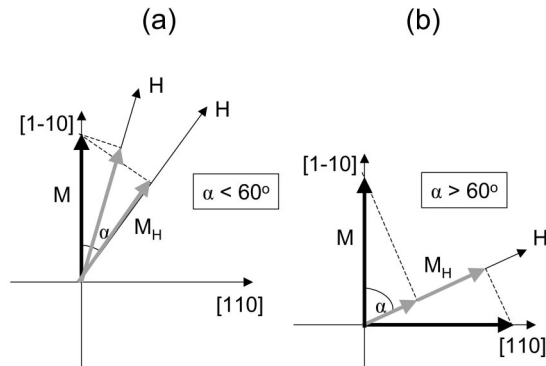


FIG. 9. A diagram illustrating the magnetization process how it is seen along the field direction at (a)  $\alpha < 60^\circ$  and (b)  $\alpha > 60^\circ$ . With increasing  $\alpha$ , the  $M$  component to the field direction ( $M_H$ ) decreases, as it is shown in (a). When the magnetization is probed at  $\alpha > 60^\circ$ , at low fields the film is magnetized along  $[1-10]$  and the magnetization projection to the field direction ( $M_H$ ) is “short.” With increasing field, the magnetization switches to  $[110]$  which results in an enlarged  $M_H$ .

initially the film is magnetized along the  $[1-10]$  direction due to the strong uniaxial anisotropy with the easy axis oriented along  $[1-10]$ . The field component acting along this direction is larger than the component acting along  $[110]$ . With increasing angle  $\alpha$ , the Kerr rotation in remanence decreases, because the projection of the magnetization (to the direction along which the magnetization is probed) decreases. Above a critical angle, i.e., at  $\alpha > 60^\circ$ , the field component along the  $[110]$  direction is strong enough (with reference to the field component along  $[1-10]$ ) to switch the magnetization from the  $[1-10]$  to  $[110]$  direction. This results in appearance of the subloop when the magnetization is probed along the field direction and the field approaches the value dominating over the uniaxial anisotropy field. Magnetization switching to the  $[110]$  direction means that a local energy minimum exists for the magnetization oriented in this way which is due to the fourfold anisotropy mentioned before. Summarizing  $\alpha > 60^\circ$ : at low fields, the projection of magnetization oriented along the  $[1-10]$  direction contributes to the MOKE signal. At higher fields, after the magnetization is switched to the  $[110]$  direction, the MOKE signal remarkably increases. This is a simple geometrical effect explained in Figs. 9(a) and 9(b). With further increase of the field the magnetization rotates towards the field direction and saturates at the field of about 0.2 T. Finally, when the magnetization is probed along  $[110]$ , no field component along the  $[1-10]$  direction results in zero Kerr effect at low fields. Only at higher fields the magnetization switches to the  $[110]$  direction and the corresponding subloop is detected.

Previously, two-step magnetization switching has been reported in epitaxial Fe thin films due to the different combination of the uniaxial and cubic anisotropies.<sup>35–38</sup> Hathaway *et al.*<sup>39</sup> observed a three-step switching in Fe films grown on  $\text{Ag}(001)$ , in a field applied at  $7^\circ$  and  $12^\circ$  from the hard axis  $[110]$ , and attributed it to the demagnetization effect. Cowburn *et al.*<sup>40</sup> reported a hysteresis loop with three jumps in ultrathin Fe films with cubic anisotropy and a weak uniaxial anisotropy. They attributed the switching to domain wall pinning and the weak uniaxial anisotropy. Based on their calculation, three-jump switching can only be observed in a narrow range of angle when the uniaxial anisotropy is greater than the domain wall pinning energy. More recently, Ambrose *et al.*<sup>16</sup> deposited  $\text{Co}_2\text{MnGe}$  films on a GaAs substrate by molecular-beam epitaxy, and found that the epitaxial films show a large magnetization along with a small magnetic anisotropy. By using the magneto-optical indicator film imaging technique and vibrating sample magnetometry (VSM), Yang *et al.*<sup>41</sup> have studied the domain patterns and magnetic anisotropy in a  $\text{Co}_2\text{MnGe}/\text{GaAs}(001)$  film at room temperature. As a result, multistep magnetic switching has been observed in their  $\text{Co}_2\text{MnGe}$  Heusler alloy films.

For the  $\text{Co}_2\text{MnSi}$  films grown on  $\text{GaAs}(001)$  we have observed the three-jump magnetization switching when the field is applied at an angle within the range from  $60^\circ$  to nearly  $90^\circ$  with respect to the  $[1-10]$  direction. We have quantitatively shown that the magnetization aligns along the easy axis  $[1-10]$  at low fields, and then switches to the  $[110]$  direction at higher fields. This is clearly seen within the MOKE hysteresis loops, which reflect two-step magnetization reversal if projected to the field direction.

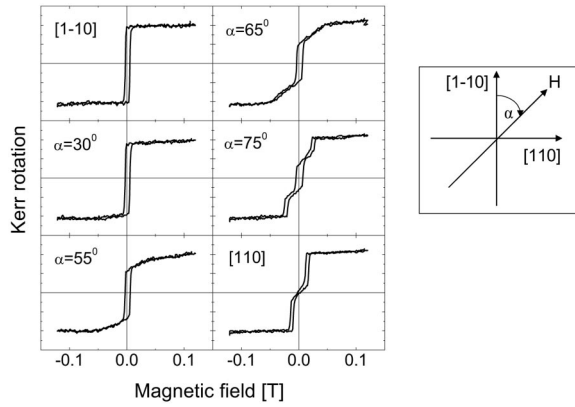


FIG. 10. Longitudinal MOKE hysteresis loops of the 60-Å  $\text{Co}_2\text{MnSi}$  film measured at RT along  $\alpha=0^\circ, 30^\circ, 55^\circ, 65^\circ, 75^\circ,$  and  $90^\circ$  in-plane azimuthal angle with respect to the  $[1-10]$  direction.

Figure 10 shows longitudinal MOKE hysteresis loops measured for the 60-Å-thick  $\text{Co}_2\text{MnSi}$  film at 300 K. The magnetization was probed in the sample plane at an angle  $\alpha$  in  $5^\circ$  steps with respect to the  $[1-10]$  direction. The only difference in comparison to the situation at 80 K (Fig. 8) concerns the narrow range of angles around  $60^\circ$  at which the magnetization prefers to follow the field direction rather than the  $[110]$  direction. The anisotropy depends on temperature, and thus is less pronounced at RT. As a consequence, when  $\alpha$  increases from  $0^\circ$  to  $60^\circ$ , the hysteresis loops become more slanted but the magnetization in remanence is the same as at 80 K. At  $\alpha \approx 60^\circ$ , at low fields the film is magnetized along  $[1-10]$ , with increasing field the magnetization does not switch to  $[110]$  as it does at 80 K, but coherently rotates to the field direction. The magnetization switches to the  $[110]$  direction only if the field is applied at larger angles ( $\alpha > 75^\circ$ ) with reference to the  $[1-10]$  direction. After switching to  $[110]$ , at higher fields, the magnetization rotates to the field direction.

Although a uniaxial anisotropy has been observed in several previous studies,<sup>35–40</sup> in particular for Fe films grown on semiconductors of the zinc-blende structure, e.g., GaAs, ZnSe, or InAs, its origin remains an open question. There have been many theoretical efforts to explain the origin of the in-plane uniaxial anisotropy. For example, it might be due to a reconstruction of the semiconducting substrates, formation of an interface alloy, or, most likely, anisotropic interfacial bonds. In the case of our  $\text{Co}_2\text{MnSi}/\text{GaAs}(001)$  films, the uniaxial anisotropy depends strongly not only on temperature but also on the film thickness. For the whole thickness range we investigated, the easy axis was found to lie in plane, and no perpendicular component of magnetization was detected. In addition, we found that the uniaxial behavior of the in-plane magnetic anisotropy persists up to about 35 bilayers (roughly 100 Å), and therefore it can not be related to any shape anisotropy of the incipient growing film. The switching field  $H_s$  is proportional to the reciprocal film thickness. Until no other direct experimental evidence is obtained, we may conclude that the uniaxial character of the GaAs unit cell, and implicitly of the interface, may bear the whole responsibility for the magnetic anisotropy we found in the  $\text{Co}_2\text{MnSi}/\text{GaAs}(001)$  system.

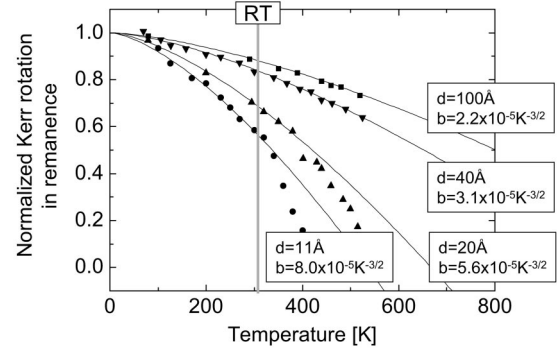


FIG. 11. Normalized Kerr rotation in remanence measured along the  $[1-10]$  direction vs temperature for the  $\text{Co}_2\text{MnSi}$  films of different thicknesses  $d$ . The results of fit to the  $M(T)=M(0)(1-bT^{3/2})$  Bloch formula at  $T < 0.6T_c$ , are included (solid lines).

Figure 11 shows the temperature dependence of the Kerr rotation in remanence measured along the  $[1-10]$  easy-axis direction for a number of films of different thickness. It is clearly seen that the magnetization depends more strongly on temperature with the decreasing film thickness. As a result, the thinner the film the smaller magnetization is detected at a finite temperature with respect to the 0 K value. In the case of our  $\text{Co}_2\text{MnSi}$  films on GaAs(001), no pronounced linear dependence of magnetization vs. temperature is observed (Fig. 11), as it is expected for the continuous films.<sup>42</sup> We found that for all of our  $\text{Co}_2\text{MnSi}$  films, the temperature dependence of the Kerr rotation in remanence can be described, at low temperatures and within reasonable limits, by the standard Bloch formula

$$M(T) = M(0)(1 - bT^{3/2}), \quad (2)$$

where  $M(0)$  and  $b$  depend on the film thickness.<sup>43</sup> We fitted the data for all our films (of different thickness) to the same formula in order to describe the temperature dependence of magnetization with one parameter  $b$ .<sup>42</sup> Due to a linear dependence of the  $b$  parameter on the reciprocal of the film thickness, its value can be found for each thickness, as it is described in details elsewhere.<sup>43</sup> Finally, the parameter  $b$  is useful to rescale, e.g., the apparent magnetic moment measured at RT to its value at 0 K (as it is described below). Actually, this can be applied to all quantities which depend on temperature in the same way as the magnetization does in order to get rid of finite size effects.

## V. X-RAY MAGNETIC CIRCULAR DICHROISM STUDY

Spin polarization at the Fermi level is related to the magnetic moments of Co and Mn. Since atomic disorder is suggested as a mechanism to reduce spin polarization, this should also have an influence on Co and Mn magnetic moments. Thus, we have studied the magnetic properties of  $\text{Co}_2\text{MnSi}$  epitaxial films up to the thickness of 85 Å, by using the element-selective x-ray magnetic circular dichroism (XMCD). Figure 12 shows the representative x-ray absorption spectra (XAS) at the Co- $L_{2,3}$  edge and corresponding XMCD difference spectra, recorded at RT, for 17-Å- (6

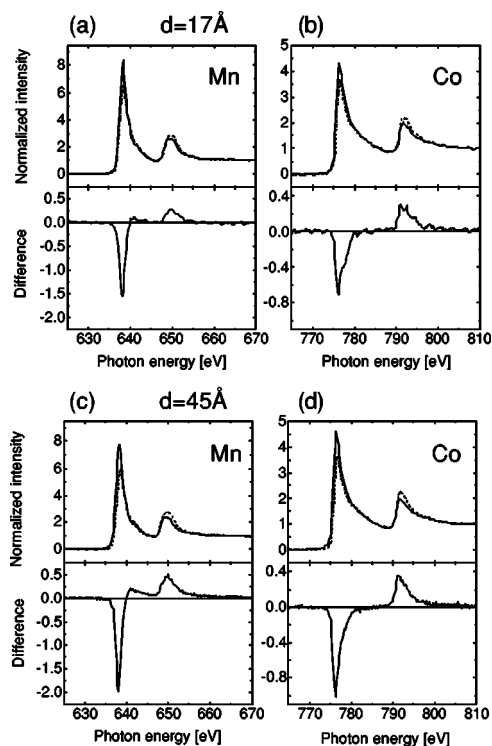


FIG. 12. X-ray-absorption spectra (top) and XMCD (bottom) at the  $L_{2,3}$  absorption edge of Mn and Co for the 17-Å- [(a) and (b)] and 45-Å- [(c) and (d)] thick  $\text{Co}_2\text{MnSi}$  films. The spectra were recorded at RT.

bilayers) and 45-Å- (close to 16 bilayers) thick  $\text{Co}_2\text{MnSi}$  films [in Figs. 12(b) and 12(d), respectively]. The XAS spectra show the two  $L_3$  and  $L_2$  resonant peaks corresponding to the  $2p_{3/2} \rightarrow 3d$  and  $2p_{1/2} \rightarrow 3d$  transitions at 776.5 and 791.5 eV, respectively, similar to the XAS spectra observed for pure metallic Co. In particular, no multiple-peak structures in the  $L_3$  region were observed as in the case of other Co-based full-Heusler alloys, e.g.,  $\text{Co}_2\text{YSn}$  ( $Y=\text{Ti, Zr, and Nb}$ ).<sup>44</sup> The lack of the multiple-peak structures cannot be attributed to a limited energy resolution. Instead, it must be explained by a different density of states (DOS) that indicates a more metallic character of the Co  $d$  band in our  $\text{Co}_2\text{MnSi}$  films compared to other (e.g.,  $\text{Co}_2\text{YSn}$ ) Heusler alloys. The XMCD signal, defined as the normalized difference in absorption between right and left polarized x rays, depends on the exchange splitting and the spin-orbit coupling of both initial core and final valence states. A clear dichroic signal was obtained at the  $L_{2,3}$  edge of Co, corresponding to a significant magnetic moment on the Co atoms in the  $\text{Co}_2\text{MnSi}$  unit cell. The XMCD intensity at the  $L_3$  edge is much larger and sharper than that at the  $L_2$  edge as in other Co intermetallic compounds.

A more precise analysis of the data is achieved by means of sum rules,<sup>45,46</sup> which link the integrated intensity differences at the  $L_2$  and  $L_3$  edges, corrected for the incomplete degree of circular polarization and the angle of incidence, to the atomic orbital and spin moments. For the application of the sum rules the absorption spectra were scaled to zero in the pre-edge region and one in the post edge. The total ab-

sorption intensity was determined by integration of the helicity-averaged spectrum after subtraction of a steplike background with steps of 0.5 eV wide and 2/3, and 1/3 height at the positions of the  $L_3$  and  $L_2$  absorption maxima, respectively. This intensity was assumed to correspond to 2.24 unoccupied  $d$  states for Co and 4.52 for Mn.<sup>25</sup> In the case of the 45 Å thick  $\text{Co}_2\text{MnSi}$  film, the application of the sum rules gives access to a magnetic spin moment of  $1.04\mu_B$  per cobalt atom, compared to the  $1.06\mu_B$  value predicted by band-structure calculations (at 0 K),<sup>47</sup> in excellent agreement with available neutron-diffraction data.<sup>48</sup> However, for other Heusler alloys (e.g.,  $\text{Co}_2\text{YSn}$ ), the magnetic moment per Co atom is known to have values ranging from 0.3 to  $1.0\mu_B$ ,<sup>49</sup> which is lower than that obtained for our  $\text{Co}_2\text{MnSi}$  films. According to the band structure calculations of the Co-based full-Heusler alloys  $\text{Co}_2\text{YZ}$ ,<sup>44</sup> it is considered that the magnetic moment on the Co atom depends strongly on the local environment, i.e., which elements are in the Y and Z sites. Moreover, it must be taken into account that our XMCD spectra were measured at RT, and thus the values of magnetic moment are underestimated (depending on the film thickness) due to the magnetic size effect. One has also to keep in mind that the electron yield is only proportional to the absorption if the x-ray penetration is large compared to the probing depth of the emitted electrons. At the strong  $L_3$  absorption maxima of the  $3d$  metals this is not exactly the case, which gives rise to so-called saturation effects. The consequence for the sum rule analysis is an underestimation of the effective spin moment, and, more pronouncedly, of the orbital moment. In the present case of  $\text{Co}_2\text{MnSi}$  films, the influence of saturation effects can be roughly estimated on the basis of the simulations presented in Ref. 28, and the atomic density of Co and Mn in  $\text{Co}_2\text{MnSi}$ . It is strongest for the thickest films of 83 Å, where it amounts to nearly 10% for the spin moment and about 25% for the orbital moment, but is negligible for the 17 Å film. The stronger absorption of Mn  $L_3$  compared to Co  $L_3$  is about compensated by the different densities of Co and Mn atoms in  $\text{Co}_2\text{MnSi}$ .

Figure 12 also shows XAS spectra at the Mn- $L_{2,3}$  edge and deduced XMCD spectra recorded at RT for the same  $\text{Co}_2\text{MnSi}$  samples for which the XAS spectra at the Co- $L_{2,3}$  edge are shown (for both 17-Å- and 45-Å-thick films, in (a) and (c), respectively). The XAS spectra show the resonant absorption lines at 638.5 and 651.4 eV for the Mn  $L_3$  and  $L_2$  edges, respectively. One can clearly find significant differences between the Mn- $L_{2,3}$  and Co- $L_{2,3}$  edge XMCD spectra shown in Fig. 12. In contrast to the XAS spectra of Co, the spectra of Mn for the  $\text{Co}_2\text{MnSi}$  films show a doublet structure at the  $L_2$  region, and a peak at  $L_3$  which is accompanied by a shoulder at higher photon energy. The doublet structure is better seen in the Mn- $L_{2,3}$  edge spectra of the thinner  $\text{Co}_2\text{MnSi}$  films (e.g., 17 and 45 Å, shown in Fig. 12), where two distinct peaks at 649.4 and 650.8 eV clearly exist. Indeed, the shape of Mn absorption spectra does not exhibit a metallic shape similar to that of Co in the  $\text{Co}_2\text{MnSi}$  films. The doublet structure, corresponding to an atomiclike behavior, has already been observed for the half-Heusler NiMnSb alloy thin films.<sup>14</sup> The multiplet peak is due to an interplay of two effects, namely, the exchange and Coulomb interactions between the core holes and unpaired electrons in the valence

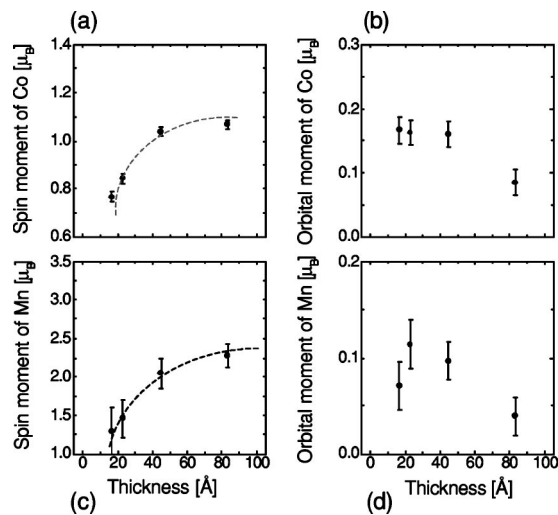


FIG. 13. Results of the sum rule application for the magnetic spin (a) and orbital (b) moments (in units of  $\mu_B$ ) of Co and Mn, measured at RT, plotted vs  $\text{Co}_2\text{MnSi}$  film thickness. Dotted lines visualize increase of the moments measured at RT with increasing film thickness. The error bars include the statistical error and part of the systematic error of the sum rule analysis.

band, and strong hybridization between the  $3d$  and surrounding electronic states. A huge negative dichroism signal was found within the  $L_3$  region, and a small positive one in the  $L_2$  region. The appearance of Mn- $L_{2,3}$  edge XMCD signals means that the Mn-Mn coupling in  $\text{Co}_2\text{MnSi}$  films is ferromagnetic, whereas it is antiferromagnetic in the bulk Mn.<sup>50</sup> On the contrary, the  $\text{Co}_2\text{MnSi}$  films have only weak Mn-Mn interaction because of a longer Mn-Mn distance, and a smaller coordination number. Therefore, Mn atoms exhibit a large magnetic moment and a ferromagnetic coupling with Co atoms in the crystal. It is, however, not possible to determine precisely the absolute value of the magnetic moment on the Mn sites in the crystal since the sum rules are well known to break down for Mn. This is due to the relatively weak spin-orbit coupling, leading to a mixing of the electronic transitions at the  $L_2$  and  $L_3$  edges. The spin moment obtained by using the sum rules could thus be underestimated even up to 30%.<sup>51</sup>

The values of the spin moment ( $m_s$ ) and orbital moment ( $m_l$ ) of Co and Mn atoms obtained at RT for the  $\text{Co}_2\text{MnSi}$  films of varying thickness are plotted in Fig. 13. The error bars shown there include the statistical error and part of the systematic error of the sum rule analysis (influence of width and position of the step function used to subtract the signal of the  $d \rightarrow s$  transition, and influence of energy range for integration). It does not include uncertainty in the degree of circular polarization, in the number of unoccupied  $3d$  states, the influence of saturation effects, or of the above mentioned energetic overlap of the absorption signal at the  $L_2$  and  $L_3$  edges of Mn. The values of  $m_s$  and  $m_l$  show a clear thickness dependence, which is, however, most likely due to the magnetic size effect. Only values extrapolated to 0 K can be used to access the theory, and allow a quantitative comparison. As it is described above, we measured the temperature dependence of magnetization for the films of varying thickness

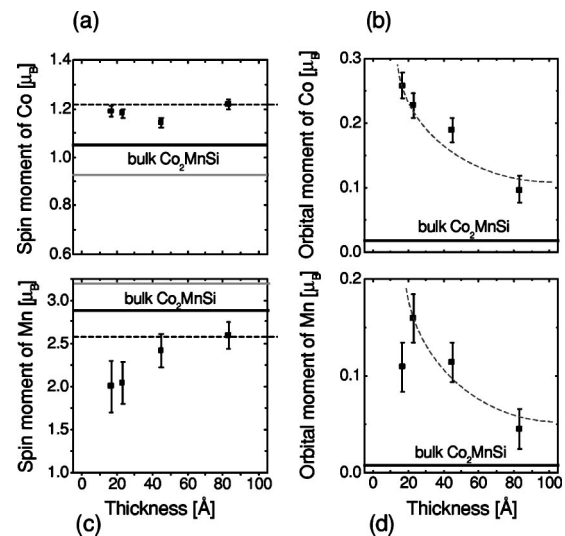


FIG. 14. The magnetic spin (a) and orbital (b) moments (in units of  $\mu_B$ ) of Co and Mn, extrapolated to 0 K, plotted vs film thickness together with theoretical values calculated for bulk  $\text{Co}_2\text{MnSi}$  (grey: Ref. 50, black: Ref. 45). Dotted lines in (a) suggest the spin moment values measured without “thin film effects.” Dotted lines in (b) show that the orbital moments decrease with increasing thickness. The error bars include the statistical error and part of the systematic error of the sum rule analysis.

with MOKE. Then we fitted the experimental points to the Bloch formula  $M(T) = M(0)(1 - bT^{3/2})$  (see Fig. 11). We found a linear dependence of the  $b$  parameter on the reciprocal of the film thickness.<sup>43</sup> Thus, for any film thickness we can determine  $b$ , and recalculate the spin and orbital moments measured at RT to their values at 0 K. The results are shown in Fig. 14. The spin moment of Co, after extrapolation to 0 K, is found to be  $1.20 \pm 0.05 \mu_B$ , which is almost independent of the film thickness. Interestingly, we note that the spin moment of Mn after extrapolation to  $T=0$  K still shows some dependence on the thickness, however, much weaker than that observed at RT. Note that taking into account saturation effects as mentioned above would lead even to a somewhat stronger dependence on film thickness.

Picozzi *et al.*<sup>47</sup> predicted theoretically for bulk  $\text{Co}_2\text{MnSi}$  alloy that  $m_s$  for Co and Mn are  $1.06 \mu_B$  and  $2.92 \mu_B$ , respectively, and a total magnetic moment of  $5.0 \mu_B$  per formula unit. The spin moment of Co ( $1.20 \mu_B$ ) we found in our films is almost 15% larger than that predicted for  $\text{Co}_2\text{MnSi}$  in the bulk form ( $1.06 \mu_B$ ). By contrast, the spin moment of Mn we found experimentally ( $\sim 2.6 \mu_B$ ) is significantly smaller than what is predicted by Picozzi *et al.* ( $2.92 \mu_B$ ). The ratio of the spin magnetic moments for Co and Mn which we obtained experimentally ( $\sim 2.17$ ) is very close to the upper limit of this parameter obtained by Schmalhorst *et al.*<sup>25</sup> for the 100-nm-thick  $\text{Co}_2\text{MnSi}$  film grown by magnetron sputtering, however, far from the 2.75 value expected from the band structure calculations.<sup>47</sup> We suggest some possible reasons for such disagreement between our experiment and theory on the Co and Mn magnetic moments. (1) As was already discussed in the previous section, the sum rule evaluations may underestimate the spin moment of Mn by about 30%. (2) As

mentioned before, magnetically dead layers formed in the surface/interface may reduce the average spin moment in particular for the thinnest films (however, this is seen for Mn only, not for Co); in particular,  $\text{MnO}_x$  formation, resulting in a presence of paramagnetic Mn ions, can be expected.<sup>25</sup> (3) A local atomic disorder, either by interchange of Co and Mn atoms or by partial occupancy of the Mn sites with Co atoms. In particular, the similar atomic radii of Co and Mn atoms encourage local atomic disorder. Assuming the existence of local atomic disorder between Co and Mn, Sasioglu *et al.*<sup>52</sup> have studied the magnetic properties of the  $\text{Co}_2\text{MnSi}/\text{GaAs}(001)$  system by using the generalized gradient approximation (GGA) band structure calculations. They found that in any case disorder results in an increased spin moment of those Co atoms which occupy the Mn site [up to  $1.56\mu_B$  (Ref. 52)]. On the other hand, those Mn atoms which occupy the Co site are antiferromagnetically coupled to the Mn atoms sitting in their normal positions, which results in a strongly reduced average moment of Mn. The magnetic moment per formula unit is also reduced in this case by about 10% in comparison to the defect-free bulk  $\text{Co}_2\text{MnSi}$ .<sup>51</sup> Very similar results were obtained recently by Picozzi *et al.*<sup>53</sup> In the case of Co-Mn swap of the order of 5–7%, they found the magnetic moment per formula unit to be reduced by exactly 10%. Hence, atomic disorder seems to play a major role for the magnetic properties of Heusler alloy films.

Our experimental findings for the  $\text{Co}_2\text{MnSi}$  alloy thin films seem to confirm theoretical predictions only qualitatively. Reduction of the Mn moment by about 10% (in comparison to the value calculated for the defect-free bulk  $\text{Co}_2\text{MnSi}$  alloy) can be explained by antiferromagnetically oriented moments of the Mn atoms sitting in the Co positions (predicted, e.g., by Sasioglu *et al.*<sup>52</sup>), or even by local precipitations of the metallic antiferromagnetic Mn. A segregated nonmagnetic surface layer of Mn, even if it was formed (see Sec. III), would have no substantial influence on the magnetic moments, which differ remarkably from the theoretical values (calculated for the defect-free bulk  $\text{Co}_2\text{MnSi}$  alloy) even in the case of very thick films. Mn segregation to the surface could only explain the decreased magnetic moment of Mn in the case of the thinnest  $\text{Co}_2\text{MnSi}$  films [see Fig. 14(c)]. The magnetic moment of the Co atoms is even increased in this case according to what is expected in the presence of Co antisites on Mn sublattice. However, within both theoretical approaches,<sup>52,53</sup> it is not easy to explain the increase of the average Co moment up to the value of  $1.20\mu_B$ , which could not result neither from Co antisites on the Mn sublattice nor from Co-Mn interchange. In addition, the magnetic moment per formula unit which we found experimentally equals to about  $5.0\mu_B$ , i.e., is very close to the theoretical value calculated for the defect-free bulk alloy. This is in contrast to the 10% decrease of the magnetic moment per  $\text{Co}_2\text{MnSi}$  formula unit which is predicted theoretically in the case of 5–7% swaps of all Co-Mn pairs.<sup>52,53</sup> The magnetic moment per formula unit which we found experimentally is not decreased with reference to the theoretical value calculated for the defect-free bulk  $\text{Co}_2\text{MnSi}$  alloy due to the magnetic moment of Co, which in the experiment amounts to  $1.20\mu_B$ , i.e., higher than the predictions of both the Sasioglu *et al.*<sup>52</sup> and Picozzi *et al.*<sup>53</sup> models in any case

of disorder that they analyzed. Thus, the question has to be addressed whether only the details of the growth process might be resulting in this higher average moment of Co, or also the details of theoretical band structure calculations might not perfectly describe the influence of disorder on the electronic properties of the Heusler alloys.

Based on the calculations by Picozzi *et al.*,<sup>47</sup> in the bulk  $\text{Co}_2\text{MnSi}$ , the orbital moments  $m_l$  are predicted to be very close to zero, about  $0.008\mu_B$  for Mn and  $0.02\mu_B$  for Co, showing that the orbital magnetic moment is quenched due to the cubic symmetry. However, as it is shown in Fig. 14, our experimental values for both the Co and Mn orbital moments  $m_l$  are significantly enhanced with respect to the theoretically predicted bulk values, even more so when considering the underestimation of the orbital moment by the sum rule analysis due to saturation effects in the total electron yield detection. Increased orbital moments have been observed previously with decreasing thickness of Co films grown on  $\text{Cu}(100)$ ,<sup>54</sup> in Co/Pd multilayers,<sup>55</sup> and Fe/Pd multilayers.<sup>56</sup> This has been interpreted in terms of the reduced coordination at the surface (or at the interface). Moreover, a giant enhancement of the orbital moment of 300% with respect to the bulk Fe value has been recently reported to occur in a thin Fe film grown on  $\text{GaAs}(001)$ .<sup>57</sup> In that case, the enhancement of  $m_l$  has been interpreted in terms of perpendicular interface anisotropy in the Fe/GaAs system. In contrast to the bulk  $\text{Co}_2\text{MnSi}$  crystals where the orbital moment is nearly completely quenched, a strong enhancement of the orbital moment occurs with decreasing thickness of our  $\text{Co}_2\text{MnSi}$  films. As is shown in Fig. 14, in the case of the 83-Å-thick film, the orbital moments of Co and Mn are  $0.10 \pm 0.02\mu_B$  and  $0.04 \pm 0.02\mu_B$ , respectively, which means that the moments are enhanced by a factor of roughly 5 compared to the bulk values predicted theoretically. According to a discussion based on second-order perturbation theory, the orbital magnetic moment of a cubic  $3d$  compound arises from the mixing either of the  $t_{2g}$  orbital, or between  $t_{2g}$  and  $e_g$  orbitals.<sup>58</sup> Therefore, when we discuss the orbital magnetic moment of a Heusler alloy, the effect of the character of the  $3d$  electrons has to be considered. It is believed that in the cubic  $3d$  compounds the orbital magnetic moment becomes larger when the  $3d$  states are more localized.<sup>58</sup> Therefore, the large orbital moment of Co and Mn atoms in the  $\text{Co}_2\text{MnSi}$  film suggests that the  $3d$  electronic states of both the Co and Mn are more localized in our films than in bulk, which may be the reason for the large orbital moments. The influence of the reduced symmetry in thin films has shown to be responsible for an increase of the orbital moment with decreasing thickness.<sup>54–56</sup> However, this is probably not the main mechanism here, since the increase of the orbital moment occurs on a much larger thickness scale than the one in Refs. 54–56.

## VI. SPIN POLARIZATION IN $\text{Co}_2\text{MnSi}$ FILMS

Now we turn to the spin-resolved photoemission spectra (SRPES) measurements of the  $\text{Co}_2\text{MnSi}$  films of varying thickness. Prior to the measurements, the films were magnetized in-plane along the [1-10] easy axis direction. Figures

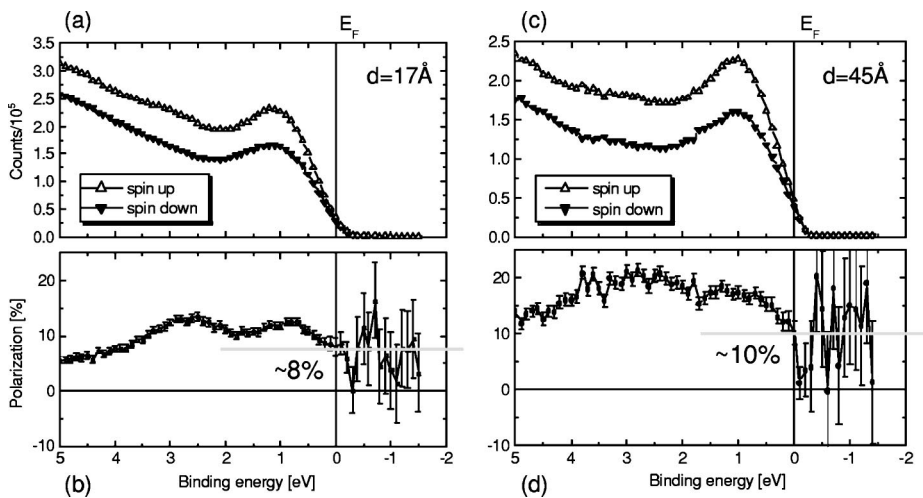


FIG. 15. (a) and (c) Spin-resolved photoemission spectra of the 17-Å- and 45-Å-thick  $\text{Co}_2\text{MnSi}/\text{GaAs}(001)$  films detected at 70 eV photon energy. Open (filled) triangles denote majority- (minority-) spin spectra. (b) and (d) Spin polarization, defined as difference between majority and minority photoemission intensities normalized to the total intensity of the spectra of (a) and (c), respectively.

15(a)–15(d) show the representative spin-resolved valence band photoemission spectra measured at RT and corresponding spin polarization for 17-Å- (6 bilayers) and 45-Å- (16 bilayers) thick  $\text{Co}_2\text{MnSi}$  films. Both spectra show the majority-spin spectrum of higher overall intensity than the minority one. A broad peak at  $\sim 0.9$  eV is suggestive of a mixture of metalliclike Co and Mn components. An absence of the more detailed band structure is related to the photoelectron energy resolution in our experiment which is estimated to be of the order of 0.5 eV. It is worth to notice that the spin-resolved photoemission spectra of NiMnSb films obtained by Zhu *et al.*<sup>59</sup> are similar to our observations. Moreover, our results are in a qualitative agreement (e.g., the peak at 0.9 eV energy which is accompanied by a signal increase towards higher binding energies) with the spin-resolved density of states (SRDOS) calculated by Picozzi *et al.*<sup>47</sup> who performed band structure calculations of bulk  $\text{Co}_2\text{MnSi}$  by means of all-electron full-potential linearized augmented plane wave (FLAPW) method.

We define the spin polarization  $P$  as difference between the intensity spectra for majority and minority spins, normalized to the total intensity,  $P = (I_{\text{up}} - I_{\text{down}}) / (I_{\text{up}} + I_{\text{down}})$ . The spin polarization corresponding to the spectra of Figs. 15(a) and 15(c) is depicted in Figs. 15(b) and 15(d), respectively. One can see that at RT the spin polarization at the Fermi energy for the 17-Å- and 45-Å-thick  $\text{Co}_2\text{MnSi}$  films is 8 and 10 %, respectively. The extrapolation to 0 K is performed exactly in the same way as that for the magnetic moments. The picture of disordered magnetic moments assumes that the atomic moments are basically independent of temperature. Then the decrease of the net magnetization is a consequence of the deviation of the atomic moments from the magnetization axis. The average deviation increases with temperature making the net magnetization smaller. Since the atomic moments are unchanged, the fundamental intra-atomic spin splitting is unchanged. This means that in the first approximation the total DOS of the system does not depend on temperature. On the other hand, since the atomic moments deviate from the axis of global magnetization, the distribution of the total DOS between spin-up and spin-down channels changes with temperature. Thus, the temperature dependence of the spin polarization at the Fermi level can be

related to the temperature dependence of the magnetization. The extrapolation results in a spin polarization of 12% almost independently of the film thickness, which is considerably smaller than the expected 100% for half-metallic ferromagnets (theoretically, the half-metallic property in several bulk Heusler alloys, such as NiMnSb and  $\text{Co}_2\text{MnSi}$ , is reasonably established). Although the magnitude of the measured polarization throughout the spectra is much smaller than the one predicted, the shape of the spectra is similar to the results obtained by Picozzi.<sup>47</sup> Recently Ritchie *et al.*<sup>60</sup> measured the spin polarization of several Heusler single crystal samples grown by the Czochralski method, using an Andreev-reflection method to detect the spin polarization. Their results indicate a polarization of 56% at 4.2 K for a  $\text{Co}_2\text{MnSi}$  single crystal sample. Very recently the spin polarization of the  $\text{Co}_2\text{MnSi}$  Heusler compound obtained by sputtering has been estimated from the resulting tunnel magnetoresistance-effect to be 61% at 10 K.<sup>25,61</sup>

There are at least two plausible explanations why the spin polarization is much smaller than predicted. The most obvious seems to be the presence of another nonstoichiometric phase not necessarily at the surface of  $\text{Co}_2\text{MnSi}$ , but rather randomly distributed over the film volume. A nonmagnetic metallic phase would add an equal contribution to the majority- and minority-spin components, effectively decreasing the polarization. However, a magnetically dead surface/interface layer seems not to be the case. The thickness dependence of the Kerr intensity (plotted in Fig. 6) suggests that for the films thicker than four bilayers not more than 0.6 ML are magnetically dead. For the films tens of bilayers thick, this cannot lead to a decrease of the spin polarization down to only 12%. A more plausible explanation relates to the local atomic disorder in the films. The following types of the local chemical disorder have to be considered: (1) Intermixing of Co and Mn and (2) partial occupancy of the Mn lattice sites by Co atoms (one can imagine local precipitations of the metallic Mn resulting in a surplus of the Co atoms). The local atomic disorder is the cause of the diminished spin polarization. This is due to the band theory applied for several Heusler alloys which predicts that the conduction gap at  $E_F$  in the minority spin states can be closed if some disorder is introduced into the crystal lattice. Recently,

by means of *ab initio* FLAPW calculations, Picozzi *et al.*<sup>53</sup> have investigated the influence of atomic disorder on the half-metallic character of Co<sub>2</sub>MnSi Heusler alloys. They found that antisite disorder on the level of a few percent (8%) of the Mn sites being occupied by Co atoms would result in the loss of the half-metallic character. With the same framework, Sasioglu *et al.*<sup>52</sup> applied the GGA band structure calculations to study the electronic structure of the bulk Co<sub>2</sub>MnSi. They found that any of the considered disorders, as low as a few percent, is capable to reduce significantly the spin polarization at  $E_F$ . For the experimentally observed disorder on the level of 10–15 % of Mn sites occupied by Co atoms, they found a spin polarization of only 20%, and a vanishing minority-spin band gap.

For example, in the case of Co<sub>2</sub>MnSi, an antisite disorder is manifested in the form of site swapping between the Co and Mn atoms. The similar atomic radii of Co and Mn atoms encourage this kind of disorder. Recently, a neutron-diffraction experiment was performed to probe disorder of the stoichiometric bulk Co<sub>2</sub>MnSi,<sup>21</sup> which shows that between 10 and 15 % of Mn sites are occupied by Co. Due to the relatively low deposition temperature we can assume that the degree of local atomic disorder in our films could be even higher in comparison to the bulk Co<sub>2</sub>MnSi sample made under optimum conditions. Thus, the spin polarization of 12% for the RT-grown thin films, in comparison to 56% for the perfect bulk sample, is not surprising. An existence of the site swapping between the Co and Mn atoms seems to be supported by the values of the magnetic moment which are in the case of Co increased and in the case of Mn decreased compared to theoretical calculations for the defect-free bulk Co<sub>2</sub>MnSi alloy. Such an evolution of magnetic moments can also be explained by a local nonstoichiometry of our films caused by the segregation of Mn atoms to the film surface, resulting, however, in the same dramatic reduction of the spin polarization. By comparing results obtained by XMCD and by spin-polarized photoelectron spectroscopy one has to keep in mind the different information depth of the two techniques. While in XMCD the exponential weighting depth is about 2 nm,<sup>28</sup> photoelectron spectra at the kinetic energies presented here probe less than 0.6 nm depth.<sup>62</sup> Thus, e.g., surface oxidation can remarkably influence the spin polarization detected in this way. In the case of our experiment, because of the long storage between film growth and XAS measurement, a small amount of MnO<sub>x</sub> could be formed. This is compatible with a decrease of the spin moment of Mn detected by XMCD with decreasing film thickness (Fig. 14), as well as with very low spin polarization detected by the photoemission method which is mostly surface sensitive. We measured SQUID for the 60-Å-thick film. The result for the magnetic moment is  $5.1\mu_B$  per formula unit. This is very close to the value predicted theoretically [ $(5.0\mu_B)$  (Ref. 47)], and very close to the value which we measured by XMCD. The point is that the magnetic moment of Co is increased in comparison to the value predicted theoretically ( $1.20\mu_B$  instead of  $1.06\mu_B$ ), whereas the magnetic moment of Mn is decreased from  $2.92\mu_B$  predicted theoretically to  $\sim 2.6\mu_B$ . Consequently, both moments separately give the values very different from those predicted theoretically, but per formula units the result is almost equal to the

theoretical one. Then, it is impossible to conclude on the oxidation at the surface from the difference between the XMCD and SQUID results. This is rather a confirmation that the surface oxidation is small if it exists, and that the values of magnetic moments are properly determined from the XMCD experiment as they fit well to the result of the SQUID analysis. Summarizing, not only an improvement in the film growth (in order to minimize any kind of the local chemical disorder), but also in detection of the spin polarization, is required. The point is that only a polarization close to 100% is predicted to improve remarkably the efficiency of the spin injection into the semiconductor.<sup>6</sup>

Finally, it has to be mentioned that although in the presented photoelectron data the detected electron momentum parallel to the film plane covers about one Co<sub>2</sub>MnSi Brillouin zone, a photoemission experiment does in general not necessarily represent a complete  $k$ -space sampling of the Brillouin zone in the perpendicular direction. The sampled range of electronic states may be further limited by dipole selection rules. This could in principle lead to a different (higher or lower) apparent spin polarization than expected from the total DOS.

## VII. SUMMARY

We have demonstrated that PLD can be used for a successful deposition of single crystalline Co<sub>2</sub>MnSi films. *In situ* RHEED and AES show that the best quality of the Co<sub>2</sub>MnSi films has been achieved after deposition at 450 K. The films exhibit in-plane uniaxial magnetic anisotropy with the easy axis of magnetization along the [1-10] direction superimposed to a fourfold anisotropy with the easy axis along the  $\langle 110 \rangle$ -in-plane directions. When the field is applied under an angle  $\alpha$  with respect to [1-10], the magnetization reversal proceeds in two steps: at low fields the magnetization is oriented along [1-10] and then switches to [110] at higher fields. This is clearly seen within the MOKE hysteresis loops, which reflect two-step magnetization process projected to the field direction. The anisotropy depends strongly on the film thickness and on temperature. Spin-resolved photoemission measurements at BESSY of the single-crystalline Co<sub>2</sub>MnSi films reveal a spin-resolved density of states that is in qualitative agreement with recent band structure calculations. However, the spin polarization of photoelectrons emerging from the sample is found to be at most 12% at room temperature, in contrast to the predicted half-metallic behavior. The spin and orbital magnetic moments we obtained by the sum rules analysis of XMCD measurements of thin Co<sub>2</sub>MnSi films at RT are strongly thickness dependent. The extrapolation to 0 K excludes the magnetic size effect which is responsible for the reduced magnetic moment at a finite temperature (with decreasing film thickness); nevertheless the moments differ from that predicted theoretically for the bulk Co<sub>2</sub>MnSi. We conclude that these discrepancies should be attributed rather to a partial chemical disorder in the Co<sub>2</sub>MnSi films than to nonmagnetic surface/interface regions.

## ACKNOWLEDGMENTS

We would like to thank Professor X. F. Jin, Professor G. H. Wu, Professor L. Sandratskii, and Mr. E. Sasioglu for

helpful discussions, and G. Kroder, B. Zada, and the BESSY staff for technical assistance. One of the authors (W. H. W.) thanks the Alexander von Humboldt Foundation for financial support.

\*Electronic address: mprzybyl@mpi-halle.mpg.de

- <sup>1</sup>H. Ohno, *Science* **181**, 951 (1998).
- <sup>2</sup>G. A. Prinz, *Science* **282**, 1660 (1998).
- <sup>3</sup>R. Fiederling, M. Keim, G. Reuscher, W. Ossau, G. Schmidt, A. Waag, and L. W. Molenkamp, *Nature (London)* **402**, 787 (1999).
- <sup>4</sup>C.-M. Hu and T. Matsuyama, *Phys. Rev. Lett.* **87**, 066803 (2001).
- <sup>5</sup>H. J. Zhu, M. Ramsteiner, H. Kostial, M. Wassermeier, H.-P. Schönherr, and K. H. Ploog, *Phys. Rev. Lett.* **87**, 016601 (2001).
- <sup>6</sup>G. Schmidt, D. Ferrand, L. W. Molenkamp, A. T. Filip, and B. J. van Wees, *Phys. Rev. B* **62**, R4790 (2000).
- <sup>7</sup>D. J. Monsma and S. S. P. Parkin, *Appl. Phys. Lett.* **77**, 720 (2000).
- <sup>8</sup>D. J. Monsma, R. Vlutters, and J. C. Lodder, *Science* **281**, 407 (1998).
- <sup>9</sup>G. A. Prinz, *Phys. Today* **48**, 58 (1995).
- <sup>10</sup>G. A. Prinz, G. T. Rado, and J. J. Krebs, *J. Appl. Phys.* **53**, 2087 (1982).
- <sup>11</sup>R. A. Groot, F. M. Mueller, P. G. van Engen, and K. H. J. Buschow, *Phys. Rev. Lett.* **50**, 2024 (1983).
- <sup>12</sup>S. Ishida, T. Masaki, S. Fujii, and S. Asano, *Physica B* **245**, 1 (1998).
- <sup>13</sup>S. Fujii, S. Sugimura, S. Ishida, and S. Asano, *J. Phys.: Condens. Matter* **2**, 8583 (1990).
- <sup>14</sup>P. Turban, S. Andrieu, B. Kierren, T. Snoeck, C. Teodorescu, and A. Traverse, *Phys. Rev. B* **64**, 134417 (2002).
- <sup>15</sup>W. Van Roy, J. De Boeck, B. Brijs, and G. Borghs, *Appl. Phys. Lett.* **77**, 4190 (2000).
- <sup>16</sup>T. Ambrose, J. J. Krebs, and G. A. Prinz, *Appl. Phys. Lett.* **76**, 3280 (2000).
- <sup>17</sup>J. W. Dong, L. C. Chen, C. J. Palmstrom, R. D. James, and S. McKernan, *Appl. Phys. Lett.* **77**, 4190 (2000).
- <sup>18</sup>J. W. Dong, L. C. Chen, J. Q. Xie, T. A. R. Muller, D. M. Carr, C. J. Palmstrom, S. McKernan, Q. Pan, and R. D. James, *J. Appl. Phys.* **88**, 7357 (2000).
- <sup>19</sup>J. W. Dong, J. Lu, J. Q. Xie, L. C. Chen, R. D. James, S. McKernan, and C. J. Palmstrom, *Physica E (Amsterdam)* **10**, 428 (2001).
- <sup>20</sup>P. J. Brown, K. U. Neumann, P. J. Webster, and K. R. A. Ziebeck, *J. Phys.: Condens. Matter* **12**, 1827 (2000).
- <sup>21</sup>M. P. Raphael, B. Ravel, Q. Huang, M. A. Willard, S. F. Cheng, B. N. Das, R. M. Stroud, K. M. Bussmann, J. H. Claassen, and V. G. Harris, *Phys. Rev. B* **66**, 104429 (2002).
- <sup>22</sup>U. Geiersbach, A. Bergmann, and K. Westerholt, *J. Magn. Magn. Mater.* **240**, 546 (2002).
- <sup>23</sup>S. Kämmerer, S. Heitmann, D. Meyners, D. Sudfeld, A. Thomas, A. Hütten, and G. Reiss, *J. Appl. Phys.* **93**, 7945 (2003).
- <sup>24</sup>L. J. Singh, Z. H. Barber, Y. Miyoshi, Y. Bugoslavsky, W. T. Branford, and L. G. Cohen, *Appl. Phys. Lett.* **84**, 2367 (2004).
- <sup>25</sup>J. Schmalhorst, S. Kämmerer, M. Sacher, G. Reiss, A. Hütten, and A. Scholl, *Phys. Rev. B* **70**, 024426 (2004).
- <sup>26</sup>Y. B. Xu, E. T. Kernoham, D. J. Freeland, A. Ercole, M. Tselepi, and J. A. C. Bland, *Phys. Rev. B* **58**, 890 (1998).
- <sup>27</sup>J. Kirschner, in *Polarized Electrons in Surface Physics*, edited by R. Feder (World Scientific, Singapore, 1985).
- <sup>28</sup>R. Nakajima, J. Stöhr, and Y. U. Idzerda, *Phys. Rev. B* **59**, 6421 (1999).
- <sup>29</sup>K. A. Kilian and R. H. Victora, *J. Appl. Phys.* **87**, 7064 (2000).
- <sup>30</sup>G. A. De Wijs and R. A. de Groot, *Phys. Rev. B* **64**, 020402 (2001).
- <sup>31</sup>T. Terashima, Y. Bando, K. Iijima, K. Yamamoto, K. Hirata, K. Hayashi, K. Kamigaki, and H. Terauchi, *Phys. Rev. Lett.* **65**, 2684 (1990).
- <sup>32</sup>S. Tanuma, C. J. Powell, and D. T. Penn, *Surf. Interface Anal.* **17**, 911 (1991).
- <sup>33</sup>C. M. Kwei, Y. F. Chen, C. J. Tung, and J. P. Wang, *Surf. Sci.* **293**, 203 (1993).
- <sup>34</sup>W. H. Gries, *Surf. Interface Anal.* **24**, 38 (1996).
- <sup>35</sup>J. M. Florczak and E. D. Dahlberg, *Phys. Rev. B* **44**, 9338 (1991).
- <sup>36</sup>J. R. Childress, R. Kergoat, O. Durand, J.-M. George, P. Galtier, J. Miltat, and A. Schuhl, *J. Magn. Magn. Mater.* **130**, 13 (1994).
- <sup>37</sup>C. Daboo, R. J. Hicken, D. E. P. Eley, M. Gester, S. J. Gray, A. J. R. Ives, and J. A. C. Bland, *J. Appl. Phys.* **75**, 5586 (1994).
- <sup>38</sup>R. P. Cowburn, S. J. Gray, J. Ferr, J. A. C. Bland, and J. Miltat, *J. Appl. Phys.* **78**, 7210 (1995).
- <sup>39</sup>K. B. Hathawy and G. A. Prinz, *Phys. Rev. Lett.* **47**, 1761 (1981).
- <sup>40</sup>R. P. Cowburn, S. J. Gray, and J. A. C. Bland, *Phys. Rev. Lett.* **79**, 4018 (1997).
- <sup>41</sup>F. Y. Yang, C. H. Shang, C. L. Chien, T. Ambrose, J. J. Krebs, G. A. Prinz, V. I. Nikitenko, V. S. Gornakov, A. J. Shapiro, and R. D. Shull, *Phys. Rev. B* **65**, 174410 (2002).
- <sup>42</sup>See, for example, M. Przybylski, *Hyperfine Interact.* **113**, 135 (1998).
- <sup>43</sup>W. H. Wang, M. Przybylski, W. Kuch, L. I. Chelaru, J. Wang, Y. F. Lu, J. Barthel, and J. Kirschner, *J. Magn. Magn. Mater.* **286**, 336 (2005).
- <sup>44</sup>A. Yamasaki, S. Imada, S. Suga, T. Kanomata, and S. Ishida, *Surf. Rev. Lett.* **9**, 955 (2002).
- <sup>45</sup>B. T. Thole, P. Carra, F. Sette, and G. van der Laan, *Phys. Rev. Lett.* **68**, 1943 (1992).
- <sup>46</sup>P. Carra, B. T. Thole, M. Altarelli, Xindong Wang, *Phys. Rev. Lett.* **70**, 694 (1993).
- <sup>47</sup>S. Picozzi, A. Continenza, and A. J. Freeman, *Phys. Rev. B* **66**, 094421 (2002).
- <sup>48</sup>P. J. Webster, *J. Phys. Chem. Solids* **32**, 1221 (1971).
- <sup>49</sup>K. R. A. Ziebeck and P. J. Webster, *J. Phys. Chem. Solids* **35**, 1 (1974).
- <sup>50</sup>R. Wu and A. J. Freeman, *Phys. Rev. B* **51**, 17 131 (1995).
- <sup>51</sup>Y. Tanemura, A. Tanaka, and T. Jo, *J. Phys. Soc. Jpn.* **65**, 1053 (1996).
- <sup>52</sup>E. Sasioglu, L. Sandratskii, and P. Bruno (unpublished).

- <sup>53</sup>S. Picozzi, A. Continenza, and A. J. Freeman, *Phys. Rev. B* **69**, 094423 (2004).
- <sup>54</sup>M. Tischer, O. Hjortstam, D. Arvanitis, J. Hunter Dunn, F. May, K. Baberschke, J. Trygg, J. M. Wills, B. Johansson, and O. Eriksson, *Phys. Rev. Lett.* **75**, 1602 (1995).
- <sup>55</sup>D. Weller, Y. Wu, J. Stöhr, M. G. Samant, B. D. Hermsmeier, and C. Chappert, *Phys. Rev. B* **49**, 12 888 (1994).
- <sup>56</sup>X. Le Cann, C. Boeglin, B. Carriere, and K. Hricovini, *Phys. Rev. B* **54**, R11157 (1996).
- <sup>57</sup>Y. B. Xu, M. Tselepi, C. M. Guertler, C. A. F. Vaz, G. Wastlbauer, and J. A. C. Bland, *J. Appl. Phys.* **89**, 7156 (2001).
- <sup>58</sup>G. van der Laan, *Phys. Rev. Lett.* **82**, 640 (1999).
- <sup>59</sup>W. Zhu, B. Sinkovic, E. Vescovo, C. Tanaka, and J. S. Moodera, *Phys. Rev. B* **64**, 060401 (2001).
- <sup>60</sup>L. Ritchie, G. Xiao, Y. Ji, T. Y. Chen, C. L. Chien, M. Zhang, J. Chen, Z. Liu, G. Wu, and X. X. Zhang, *Phys. Rev. B* **68**, 104430 (2003).
- <sup>61</sup>S. Kämmerer, A. Thomas, A. Hütten, and G. Reiss, *Appl. Phys. Lett.* **85**, 79 (2004).
- <sup>62</sup>R. Miranda, D. Chandesaris, and J. Lecante, *Surf. Sci.* **130**, 269 (1983).